International Journal of Heat and Mass Transfer 52 (2009) 2660–2666

Contents lists available at ScienceDirect

International Journal of Heat and Mass Transfer

journal homepage: www.elsevier.com/locate/ijhmt

# Micro-scale thermo-fluidic transport in two immiscible liquid layers subject to combined electroosmotic and pressure-driven transport

Anirban Garai, Suman Chakraborty *

*Department of Mechanical Engineering, Indian Institute of Technology, Kharagpur 721 302, India*

ARTICLE INFO

*Article history:*
Received 25 October 2008
Received in revised form 25 November 2008
Available online 21 February 2009

ABSTRACT

A theoretical analysis is presented for fully developed convective heat transfer in two immiscible fluid layers confined within parallel plate microchannels subject to combined effects of axial pressure gradients and imposed electrical fields. Assuming desperate zeta potentials at the interfaces thus formed, closed-form expressions are derived for the velocity and temperature distributions under fully developed conditions, with uniform wall heat flux boundary conditions. For the heat transfer analysis, the viscous dissipation effects are neglected as compared to the Joule heating effects. Results are subsequently obtained for different ranges of the ratios of various electrical properties of the two fluid layers and various relative strengths of the ratios of the electrical fields and the imposed pressure gradients. These results demonstrate the effects of the applied electric fields and pressure gradients, presence of external heat source or sink and interfacial positions on the temperature distributions in the two layers and the corresponding Nusselt numbers.



## 1. Introduction

Microfluidic transport plays an important role in several areas of biotechnological, biomedical and biochemical process engineering and the cooling of micro-electronic devices. In many of these applications, the fluid flow is effectively controlled by employing pressure gradients, electrical fields, or their suitable combinations. Amongst the various flow actuating mechanisms, flow augmentation and control through electroosmosis appears to be an attractive proposition in microfluidic systems [1–3], because of non-mechanical pumping and valveless operation, dispersion-free velocity profile, and inherent compatibilities with the micro-electronic circuitry.

The fundamental principle of electroosmosis [4] lies in the fact that when a solid is in contact with an electrolyte, the chemical state of the surface is generally altered, typically either by ionization of covalently bound surface groups or by ion adsorption. As a result, the surface inherits a charge while counterions are released into the liquid. The magnitude of the surface charge depends on the acidic or basic strengths of the surface groups and on the pH of the solution [5]. Despite the overall liquid being electrically neutral, an electrostatic force of attraction develops between the surface charges and the oppositely charged ions (counterions) in the liquid. Thus, a counterion concentration gradient establishes within the liquid, with a higher concentration near the solid surface and a lower concentration in the far-stream. On the other hand, the coion concentration near the surface is lower than that in the bulk liquid far away from the same, due to electrostatic repulsion. As a consequence, there is a net abundance of counterions close to the surface, which effectively balances the total charge of surface coions. Immediately next to the charged surface, a layer of immobilized counterions is present, which is known as the compact layer or the Stern layer or the Helmholtz layer. From the compact layer to the electrically neutral bulk liquid, the net charge density gradually reduces to zero. The layer of mobile ions beyond the Stern layer is called the Gouy–Chapman layer. These two layers are separated by a shear plane. The potential at this shear plane is known as the zeta potential ($\zeta$). The region encompassing the Stern layer and the Gouy–Chapman layer, over which the ionic charge density gradients are present, is also known as the electrical double layer (EDL) The characteristic thickness of the EDL is known as the Debye length ($\lambda$), which is the length from the shear plane over which the EDL potential reduces to ($1/e$) of $\zeta$. In presence of the EDL potential and the consequent charge density field, if a voltage is applied along the microchannel axis, fluid elements located within the diffuse EDL move under the action of electrostatic forces. Due to a cohesive nature of the hydrogen bonding in the polar solvent molecules, the entire buffer solution is pulled, generating a net electrokinetic body force on the bulk fluid, which is a combined function of the charge density distribution and the imposed electrical field. Fluid flows actuated by this kind of body forces are typically termed as electroosmotic flows, which form the basis of many microfluidic devices and systems of contemporary relevance.

* Corresponding author.
*E-mail address:* suman@mech.iitkgp.ernet.in (S. Chakraborty).

0017-9310/$ - see front matter © 2009 Elsevier Ltd. All rights reserved.
doi:10.1016/j.ijheatmasstransfer.2008.12.016

**Nomenclature**

| | |
|---|---|
| $C_p$ | specific heat capacity |
| $e$ | electronic charge |
| $E$ | external electric field (axial) |
| $h$ | heat transfer coefficient |
| $H$ | distance between the two plates |
| $k$ | thermal conductivity |
| $k_b$ | Boltzmann constant |
| $Nu$ | Nusselt number |
| $p$ | pressure |
| $Q$ | volume flow rate |
| $T$ | absolute temperature |
| $u$ | flow velocity |
| $q''$ | heat flux per unit width |
| $n_\infty$ | ionic number concentration in the bulk solution |
| $z$ | valence of ion |
| $\alpha$ | thermal diffusivity |
| $\phi$ | electric potential |
| $\kappa$ | Debye–Hückel parameter |
| $\varepsilon$ | permittivity |
| $\zeta_1$ | zeta potential at bottom wall |
| $\zeta_2$ | zeta potential at interface from lower fluid |
| $\zeta_3$ | zeta potential at interface from upper fluid |
| $\zeta_4$ | zeta potential at top wall |
| $\mu$ | viscosity |
| $\rho$ | density |
| $\rho_e$ | electric charge density |
| $\sigma$ | electrical conductivity |

*Subscripts*

| | |
|---|---|
| 1 | lower fluid |
| 2 | upper fluid |
| $w$ | wall |
| $b$ | bulk mean |

A key factor that determines the success of electroosmotic pumping through microchannels is the ability to develop sufficiently high concentration of dissociated ions close to the fluid–solid interface. However, some fluids, typically the poorly conductive nonpolar ones, cannot form sufficient interfacial charge density gradients to ensure electroosmotic pumping on application of the external electric fields. Such fluids, however, may be electroosmotically driven in an indirect manner, by forming an immiscible layer with another conducting fluid, so that a transverse transport of axial momentum across the two layers can take place through viscous action. An external pressure gradient may simultaneously be imposed on the system to modulate the flow.

Several research investigations have been reported in the literature on the analysis of fluid flow in two immiscible fluid layers confined in parallel plate microchannels, subject to either electroosmotic or pressure-driven fluidic actuation mechanisms, or their suitable combinations [6–10]. Such configurations would ideally be suited to constitute efficient microchannel heat sinks as well, since local thermo-fluidic control could be achieved by manipulating the geometrical and flow characteristics of the individual fluid layers. Despite such potential benefits, however, a theoretical analysis of heat transfer in immiscible fluid layers subject to combined electroosmotic and pressure-driven transport mechanisms is yet to be reported in the literature.

Aim of the present work, accordingly, is to provide a detailed analysis of fully developed convective heat transfer in two immiscible fluid layers confined within parallel plate microchannels (Fig. 1), and subject to combined effects of axial pressure gradients and imposed electrical fields. Assuming desperate zeta potentials at the three interfaces thus formed, closed-form expressions are derived for the velocity and temperature distributions under fully developed conditions, with uniform wall heat flux boundary conditions. Utilizing these expressions, the effects of the applied electric fields and pressure gradients, viscosity ratios, thermal diffusivity ratios and interfacial positions on the temperature distributions in the two layers and the corresponding Nusselt numbers are demonstrated in details.

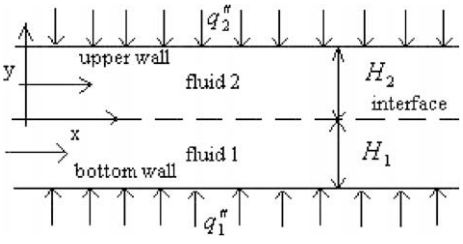


**Fig. 1.** Two immiscible fluid layers in a microchannel.

## 2. Mathematical modeling

### 2.1. Description of the physical problem

Fig. 1 depicts a schematic view of the considered model of two immiscible fluid layers of depth $H_1$ and $H_2$ in a parallel plate microchannel of total depth $H$. The two fluids are assumed to be of disparate thermo-physical properties. The electrical conductivity of the bottom fluid is considered to be higher than that of the fluid constituting the upper layer. The fluid flow is taken to be actuated by a combination of axial electric fields and pressure gradients, for generalization.

For mathematical modelling of the physical problem, following simplified assumptions are made:

(a) The fluid flow is steady, incompressible, Newtonian, and laminar [11,12],
(b) the flow is fully developed,
(c) viscous dissipation effects are negligible as compared to the Joule heating effects [13],
(d) the interface between the two immiscible fluids is planar,
(e) the fluid–fluid interface permits an accumulation of charges, resulting in the possible development of a local electrical potential,
(f) thermo-physical properties of the fluid are temperature-invariant, over the ranges of temperature being encountered,
(g) there is no overlapping of the EDLs, so that the Poisson–Boltzmann theory of potential distribution holds [14–16].

### 2.2. Electrical potential distribution

Considering the system to be in equilibrium with no macroscopic advection/diffusion of ions, the solid surface to be microscopically homogeneous and the applicability of far-stream boundary conditions at the centreline of each conducting fluid layer, the probability of finding an ion at a particular point within

the EDL can estimated to be proportional to the Boltzmann factor, $e^{-ze\phi/k_bT}$. For any binary fluid consisting of two kinds of ions of equal and opposite charge $z^+$and $z^-$, the number of ions of each type can be described by the Boltzmann distribution [4], given as $n^- = n_\infty e^{ze\phi/k_bT}$ and $n^+ = n_\infty e^{-ze\phi/k_bT}$.This distribution of ionic concentration is considered to be valid when there is no axial gradient of the ionic concentration within the microchannel and the flow Peclet number is sufficiently small, which are considered to be appropriate for the present study. The net charge density in a unit volume of the fluid, in such cases, is given as

$$\rho_e = (n^+ - n^-)ze = -2n_\infty ze \sinh(ze\phi/k_bT) \tag{1}$$

A solution for the electroosmotic potential distribution can be readily obtained by employing the Poisson–Boltzmann equation, which is of the form [4]:

$$\nabla^2\phi = -\frac{\rho_e}{\varepsilon} \tag{2}$$

With a one-dimensional distribution of the induced potential, Eq. (2) assumes the following form:

$$\frac{d^2\phi}{dy^2} = -\frac{\rho_e}{\varepsilon} \tag{3}$$

Eqs. (1) and (3) can be combined together to yield

$$\frac{d^2\phi}{dy^2} = \frac{2n_\infty ze}{\varepsilon}\sinh\left(\frac{ze}{k_bT}\phi\right) \tag{4}$$

With the Debye–Hückel linearization [4] approximation (i.e., sinh $(ze\phi/k_bT)$ is approximated as $ze\phi/k_bT$), which is a reasonably accurate assumption for the cases in which $|ze\phi/k_bT| < 1$, Eq. (4) can be re-written as

$$\frac{d^2\phi}{dy^2} = \frac{2n_\infty ze}{\varepsilon}\left(\frac{ze}{k_bT}\phi\right) = \kappa^2\phi, \quad \text{say} \tag{5}$$

where $\kappa = \sqrt{\frac{2n_\infty (ze)^2}{\varepsilon k_bT}}$ .Since in this model there are two fluid layers, the respective governing equations for electrical potential distribution become

$$\frac{d^2\phi_1}{dy^2} = \kappa_1^2\phi_1 \text{ for } -H_1 \leqslant y \leqslant 0 \tag{6a}$$

$$\frac{d^2\phi_2}{dy^2} = \kappa_2^2\phi_2 \text{ for } 0 \leqslant y \leqslant H_2 \tag{6b}$$

The solutions of the Eqs. (6a) and (6b) can be obtained as

$$\phi_1 = C_1e^{-\kappa_1 y} + C_2e^{\kappa_1 y} \text{ for } -H_1 \leqslant y \leqslant 0 \tag{7a}$$

$$\phi_2 = C_1'e^{-\kappa_2 y} + C_2'e^{\kappa_2 y} \text{ for } 0 \leqslant y \leqslant H_2 \tag{7b}$$

The integration constants $C_1$, $C_2$, $C_1'C_2'$ can be calculated by using the following boundary conditions:

$$(i) \text{ at } y = H_2,\ \phi_2 = \zeta_4, \quad (ii) \text{ at } y = 0,\ \phi_2 = \zeta_3,$$
$$(iii) \text{ at } y = 0,\ \phi 1 = \zeta_2, \quad (iv) \text{ at } y = -H_1, \phi_1 = \zeta_1 \tag{8a-d}$$

These give the following induced potential distributions within the two fluid layers:

$$\phi_1 = \frac{\zeta_2\sinh\{\kappa_1(y+H_1)\} - \zeta_1\sinh(\kappa_1 y)}{\sinh(\kappa_1 H_1)} \text{ for } -H_1 \leqslant y \leqslant 0 \tag{9a}$$

$$\phi_2 = \frac{\zeta_4\sinh(\kappa_2 y) - \zeta_3\sinh\{\kappa_2(y-H_2)\}}{\sinh(\kappa_2 H_2)} \text{ for } 0 \leqslant y \leqslant H_2 \tag{9b}$$

### 2.3. Velocity field

A combination of the electrokinetic forces and the driving pressure gradients, gives rise to the steady state velocity distribution within the microchannel, which can be obtained by solving the Navier–Stokes equation, described as

$$\rho(\vec{u}\cdot\vec{\nabla})\vec{u} = -\vec{\nabla}p + \mu\nabla^2\vec{u} + \vec{F} \tag{10}$$

where $\vec{F}$ is the net body force per unit volume that acts on the fluid. We assume the flow to be fully developed, so that there is no velocity gradient along the axial ($x$) direction. Further, since the channel is considered to be of large lateral extent as compared to its transverse dimensions, velocity gradients out of the plane of Fig. 1 can also be neglected. These considerations, coupled with the equation of mass conservation (continuity equation), lead to the following conditions, with $\vec{F} = \rho_e(\vec{E} - \vec{\nabla}\phi)$:

$$-\frac{dp}{dx} + \mu\frac{d^2u}{dy^2} + \rho_e E = 0 \tag{11}$$

It is important to mention here that the net body force is fundamentally a combined effect of the potential distributions due to the induced (EDL) and the applied electrical field. However, for a fully developed flow considered in the present analytical study, only axial components of the velocity profiles are important (transverse velocity component is identically equal to zero), which depend on the body force along the axial direction only. Since the EDL induced potential gradient acts along the transverse ($y$) direction, the only component of the electrical field that influences the velocity profile through an axially acting body force is due to the applied electric field, resulting in the simplified form as given by Eq. (11).For the flow configurations depicted in Fig. 1, Eq. (11) can be re-written with the aid of Eq. (2) as

$$0 = -\frac{dp}{dx} + \mu_1\frac{d^2u_1}{dy^2} - E\varepsilon_1\frac{d^2\phi_1}{dy^2} \text{ for } -H_1 \leqslant y \leqslant 0 \tag{11a}$$

$$0 = -\frac{dp}{dx} + \mu_2\frac{d^2u_2}{dy^2} - E\varepsilon_2\frac{d^2\phi_2}{dy^2} \text{ for } 0 \leqslant y \leqslant H_2 \tag{11b}$$

Integrating Eqs. (11a) and (11b), the velocity distributions can be obtained in the following form:

$$u_1 = \frac{1}{\mu_1}\left(\frac{dp}{dx}\right)\frac{y^2}{2} + \frac{E\varepsilon_1}{\mu_1}\phi_1 + C_3y + C_4 \quad \text{for } -H_1 \leqslant y \leqslant 0 \tag{12a}$$

and

$$u_2 = \frac{1}{\mu_2}\left(\frac{dp}{dx}\right)\frac{y^2}{2} + \frac{E\varepsilon_2}{\mu_2}\phi_2 + C_3'y + C_4' \quad \text{for } 0 \leqslant y \leqslant H_2 \tag{12b}$$

The integration constants can be evaluated by using the following boundary conditions:

$$(i) \text{ at } y = H_2,\ u_2 = 0, \quad (ii) \text{ at } y = -H_1 u_1 = 0,$$
$$(iii) \text{ at } y = 0, u1 = u_2 \text{ and}, \quad (iv) \text{ at } y = 0,\ \mu_1\frac{du_1}{dy} = \mu_2\frac{du_2}{dy} \tag{13}$$

These lead to the following expressions for the integration constants:

$$C_3 = \frac{\left[\frac{1}{\mu_1}\left(\frac{dp}{dx}\right)\frac{H_1^2}{2} - \frac{1}{\mu_2}\left(\frac{dp}{dx}\right)\frac{H_2^2}{2}\right] + \left[\frac{E\varepsilon_1}{\mu_1}(\zeta_1-\zeta_2) - \frac{E\varepsilon_2}{\mu_2}(\zeta_4-\zeta_3)\right] - KH_2}{H_1 + \frac{\mu_1}{\mu_2}H_2}$$

$$K = \frac{E\varepsilon_1}{\mu_2}\frac{\zeta_2\kappa_1\cosh(\kappa_1H_1) - \zeta_1\kappa_1}{\sinh(\kappa_1H_1)} - \frac{E\varepsilon_2}{\mu_2}\frac{\zeta_4\kappa_2 - \zeta_3\kappa_2\cosh(\kappa_2H_2)}{\sinh(\kappa_2H_2)}$$

$$C_3' = \frac{\mu_1}{\mu_2}C_3 + K$$

$$C_4 = C_3H_1 - \frac{E\varepsilon_1}{\mu_1}\zeta_1 - \frac{1}{\mu_1}\left(\frac{dp}{dx}\right)\frac{H_1^2}{2}$$
$$C_4' = \frac{E\varepsilon_1\zeta_2}{\mu_1} - \frac{E\varepsilon_2\zeta_3}{\mu_2} + C_4 \quad (13a\text{-}e)$$

### 2.4. Volume flow rates

The volume flow rates per unit width can be evaluated by integrating the velocity profiles in the two fluid layers, as

$$Q_1 = \int_{-H_1}^{0} u_1 dy = \frac{\left(3E\varepsilon_1\zeta_2 e^{(\kappa_1H_1)^2} + 3E\varepsilon_1\zeta_2 - 6E\varepsilon_1\zeta_1 e^{(\kappa_1H_1)} - 6E\varepsilon_1\zeta_2 e^{(\kappa_1H_1)} - 3C_3H_1^2\sinh(\kappa_1H_1)\mu_1\kappa_1 e^{(\kappa_1H_1)} + \frac{dp}{dx}H_1^3\sinh(\kappa_1H_1)\kappa_1 e^{(\kappa_1H_1)} + 3E\varepsilon_1\zeta_1 e^{(\kappa_1H_1)^2} + 3E\varepsilon_1\zeta_1 + 6C_4H_1\sinh(\kappa_1H_1)\mu_1\kappa_1 e^{(\kappa_1H_1)}\right)}{6\sinh(\kappa_1H_1)\mu_1\kappa_1 e^{(\kappa_1H_1)}} \quad (14a)$$

$$Q_2 = \int_{0}^{H_2} u_2 dy = \frac{\left(-6E\varepsilon_2\zeta_3 e^{(\kappa_2H_2)} + 3E\varepsilon_2\zeta_3 + 3E\varepsilon_2\zeta_3 e^{(\kappa_2H_2)^2} - 6E\varepsilon_2\zeta_4 e^{(\kappa_2H_2)} + 3C_3'H_2^2\sinh(\kappa_2H_2)\mu_2\kappa_2 e^{(\kappa_2H_2)} + \frac{dp}{dx}H_2^3\sinh(\kappa_2H_2)\kappa_2 e^{(\kappa_2H_2)} + 3E\varepsilon_2\zeta_4 e^{(\kappa_2H_2)^2} + 3E\varepsilon_2\zeta_4 + 6C_4'H_2\sinh(\kappa_2H_2)\mu_2\kappa_2 e^{(\kappa_2H_2)}\right)}{6\sinh(\kappa_2H_2)\mu_2\kappa_2 e^{(\kappa_2H_2)}} \quad (14b)$$

### 2.5. Heat transfer characteristics

Considering the derived velocity profiles, the energy conservation equation can be employed to obtain the expressions for temperature profiles in the two fluid layers. In the two fluid layers, the energy equation takes the following simplified forms:

$$\rho_1 C_{p_1}\left(u_1\frac{\partial T_1}{\partial x}\right) = k_1\frac{d^2T_1}{dy^2} + \sigma_1E^2 \text{ for } -H_1 \leqslant y \leqslant 0 \quad (15a)$$

$$\rho_2 C_{p_2}\left(u_2\frac{\partial T_2}{\partial x}\right) = k_2\frac{d^2T_2}{dy^2} + \sigma_2E^2 \text{ for } 0 \leqslant y \leqslant H_2 \quad (15b)$$

For a constant wall heat flux boundary condition and with the assumption of symmetric thermal boundary conditions at the two walls, the thermally fully developed state implies

$$\frac{\partial T_1}{\partial x} = \frac{\partial T_2}{\partial x} = \frac{dT_b}{dx} = \frac{dT_w}{dx} = \text{constant} \quad (16)$$

Accordingly, one may integrate Eqs. (15a) and (15b), to yield

$$(T_1 - T_w) = \left(\frac{y^4}{24\mu_1}\frac{dp}{dx} + \frac{E\varepsilon_1\phi_1}{\mu_1\kappa_1^2} + C_3\frac{y^3}{6} + C_4\frac{y^2}{2}\right)\frac{\frac{dT_b}{dx}}{\alpha_1} - \frac{\sigma_1E^2y^2}{2k_1} + C_5y + C_6 \text{ for } -H_1 \leqslant y \leqslant 0 \quad (17a)$$

$$(T_2 - T_w) = \left(\frac{y^4}{24\mu_2}\frac{dp}{dx} + \frac{E\varepsilon_2\phi_2}{\mu_2\kappa_2^2} + C_3'\frac{y^3}{6} + C_4'\frac{y^2}{2}\right)\frac{\frac{dT_b}{dx}}{\alpha_2} - \frac{\sigma_2E^2y^2}{2k_2} + C_5'y + C_6' \text{ for } 0 \leqslant y \leqslant H_2 \quad (17b)$$

The integration constants can be evaluated by using the following matching conditions:

$$(i) \text{ at } y = -H_1,\ T_1 = T_w \ (ii) \text{ at } y = H_2,\ T_2 = T_w \text{ at } y = 0,\ T_1 = T_2 \text{ at } y = 0, \quad k_1\frac{dT_1}{dy} = k_2\frac{dT_2}{dy} \quad (18)$$

It is important to note here that the parameter $T_w$ is not a known boundary parameter, since specification of the heat flux ensures that the gradient of $T$ (Neumann boundary condition) rather than $T$ itself may be prescribed at the walls. In that respect, expressions 18(i, ii) merely act as trivial conditions to be always satisfied at the walls (irrespective of any arbitrary exact variations in $T_w$), but not as a true boundary condition. The constants of integration, thus, can be obtained as

$$C_5 = \frac{K\frac{dT_b}{dx} - \left(\frac{\sigma_1E^2H_1^2}{2k_1} - \frac{\sigma_2E^2H_2^2}{2k_2}\right) + \left(\frac{E\varepsilon_2\zeta_3\frac{dT_b}{dx}}{\mu_2\kappa_2^2\alpha_2} - \frac{E\varepsilon_1\zeta_2\frac{dT_b}{dx}}{\mu_1\kappa_1^2\alpha_1}\right) - K_1H_2}{H_1 + \frac{k_1}{k_2}H_2} \quad (19)$$

where

$$K = \left(\frac{\frac{dp}{dx}H_1^4}{24\mu_1\alpha_1} - \frac{\frac{dp}{dx}H_2^4}{24\mu_2\alpha_2}\right) + \left(\frac{E\varepsilon_1\zeta_1}{\mu_1\kappa_1^2\alpha_1} - \frac{E\varepsilon_2\zeta_4}{\mu_2\kappa_2^2\alpha_2}\right) - \left(\frac{C_3H_1^3}{6\alpha_1} + \frac{C_3'H_2^3}{6\alpha_2}\right) + \left(\frac{C_4H_1^2}{2\alpha_1} - \frac{C_4'H_2^2}{2\alpha_2}\right)$$
$$K_1 = \frac{Ek_1\varepsilon_1\frac{dT_b}{dx}}{k_2\mu_1\alpha_1\kappa_1}\frac{\zeta_2\cosh(\kappa_1H_1) - \zeta_1}{\sinh(\kappa_1H_1)} - \frac{E\varepsilon_2\frac{dT_b}{dx}}{\mu_2\alpha_2\kappa_2}\frac{\zeta_4 - \zeta_3\cosh(\kappa_2H_2)}{\sinh(\kappa_2H_2)}$$
$$C_5' = \frac{k_1}{k_2}C_5 + K_1$$
$$C_6 = -\left(\frac{\frac{dp}{dx}H_1^4}{24\mu_1} + \frac{E\varepsilon_1\zeta_1}{\mu_1\kappa_1^2} - C_3\frac{H_1^3}{6} + C_4\frac{H_1^2}{2}\right)\frac{\frac{dT_b}{dx}}{\alpha_1} + \frac{\sigma_1E^2H_1^2}{2k_1} + C_5H_1$$
$$C_6' = \left(\frac{E\varepsilon_1\zeta_2}{\mu_1\kappa_1^2\alpha_1} - \frac{E\varepsilon_2\zeta_3}{\mu_2\kappa_2^2\alpha_2}\right)\frac{dT_b}{dx} + C_6 \quad (19a\text{-}e)$$

Eqs. 17a, 17b, and 19 together constitute the solution of the temperature distribution in the two fluid layers.

### 2.6. Nusselt number calculation

Utilizing the velocity and temperature distributions, the bulk mean flow temperature can be calculated as

$$(T_b - T_w) = \frac{\int_{-H_1}^{0}\rho_1C_{p_1}u_1(T_1 - T_w)dy + \int_{0}^{H_2}\rho_2C_{o_2}u_2(T_2 - T_w)dy}{\int_{-H_1}^{0}\rho_1C_{p_1}u_1dy + \int_{0}^{H_2}\rho_2C_{p_2}u_2dy}$$

Utilizing the interfacial conditions at the walls as

$$h_1(T_w - T_b) = k_1\left.\frac{d(T_w - T)}{dy}\right|_{y=-H_1} \quad (21a)$$

$$h_2(T_w - T_b) = -k_2\left.\frac{d(T_w - T)}{dy}\right|_{y=H_2} \quad (21b)$$

the Nusselt number can be obtained as

$$Nu_1 = \frac{2h_1(H_1 + H_2)}{k_1} \quad (22a)$$

$$Nu_2 = \frac{2h_2(H_1+H_2)}{k_2} \tag{22b}$$

Employing these relationships, a closed-form expression for the Nusselt number may be derived. The expression is somewhat involved, but may easily be obtained through the employment of a suitable symbolic mathematics software. The temperature gradient along the flow direction can be calculated by overall energy balance in a control volume of unit width assuming $q_2'' = q_1'' = q''$ as

$$(\rho_1 C_{p1} Q_1 + \rho_2 C_{p2} Q_2)\frac{dT_b}{dx} = 2q'' + (H_1\sigma_1 + H_2\sigma_2)E^2 \tag{23}$$

## 3. Results and discussions

The analytical model developed in this study is simulated by using the following choices of thermo-physical properties, for the sake of illustration: by $\frac{\mu_2}{\mu_1} = 20\frac{\rho_2}{\rho_1} = 1\frac{k_2}{k_1} = 0.1$ and $\frac{C_{p_2}}{C_{p_1}} = 1$. The parameter $\kappa$ is evaluated at a reference temperature of 298 K. These simulation studies are executed with reference to the following non-dimensional parameters: $P = \frac{\frac{E\varepsilon_1}{\mu_1}\left(\frac{\zeta_1+\zeta_2}{2}\right)+\frac{E\varepsilon_2}{\mu_2}\left(\frac{\zeta_3+\zeta_4}{2}\right)}{\left(\frac{H_1^2}{2\mu_1}+\frac{H_2^2}{2\mu_2}\right)\left(\frac{dp}{dx}\right)}$, which is a measure of the relative significance of electroosmotic force relative to the force on account of the driving pressure gradients, and $S = \left(\frac{2q''}{\sigma_1E^2H_1+\sigma_2E^2H_2}\right)$,which is measure of relative dominance of the external heat transfer rate with respect to the rate of Joule heating. The electrical conductivity ratio is varied for different simulations, so as to obtain a detailed qualitative and quantitative insight regarding the effect of the same on the overall heat transfer characteristics.

Fig. 2 depicts typical velocity profiles in the two fluid layers with varying P, when the interfacial position is assumed to be located exactly at midway between the two plates. The electrical properties are taken in accordance with the following: $\frac{\varepsilon_2}{\varepsilon_1} = 0.5$, $\zeta_1$ = $\zeta_2$, $\zeta_3$ = $\zeta_4$ = $0.5\zeta_1$, and $\frac{\sigma_2}{\sigma_1} = 0.1$. Because of substantially lower viscosity of the lower fluid layer as compared to the upper one, a substantially higher interfacial velocity gradient exists in the bottom fluid, to satisfy the requirements of shear-stress continuity. It can also be observed from Fig. 2 that higher values of P are associated with higher magnitudes of the flow velocities. This can be attributed to the fact that for a given imposed pressure gradient, higher values of P imply stronger electroosmotic body forces, giving rise to augmented flow strengths. On the other hand, negative values of P imply opposing influences of the applied electric field and the imposed pressure gradient. This is equivalent to the imposition of an adverse pressure gradient on an electroosmotically driven flow-feld, resulting in reduced strengths of flow (including possibilities of backflow; for example see the curve corresponding to P = -0.05 in Fig. 2).

Fig. 3 depicts typical temperature profiles in the two fluid layers with varying $S$ and with $P = \pm 0.05$, all other parameters remaining the same as those being employed to obtain Fig. 2. The case with $S = -1$represents an external cooling from the channel walls, so that the fluid temperature remains greater than the wall temperature at all locations. When $S = 0$, the external heat fluxes at the channel walls are effectively zero. Under these conditions, the Joule heating effects in the lower fluid layer tend to increase its temperatures to a perceptible extent. The upper layer being electrically much less conductive, there is no substantial Joule heating within the same. However, because of the transverse heat conduction effects, and aggravated by the fact that the heat generated in the bottom layer cannot easily escape to the immediate surroundings by penetrating through the wall without any external aid; this heat encounters the least resistance to be propagated upwards. This gives rise to a locally decreasing vertical temperature gradient

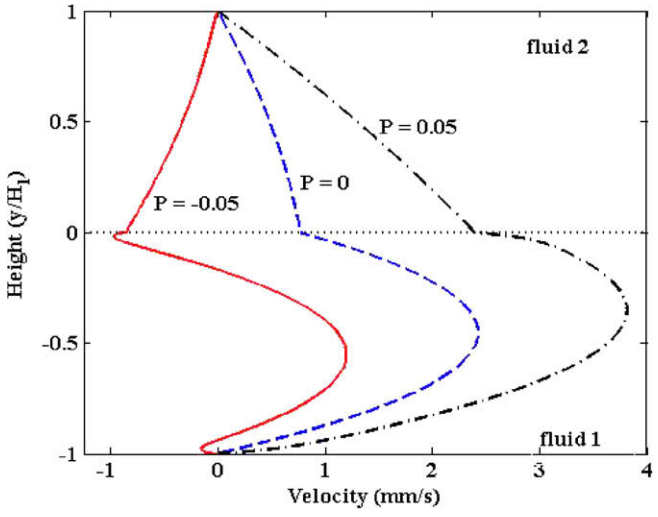


**Fig. 2.** Representative velocity profiles in the two fluid layers, for different values of P, taking equal thicknesses of the two fluid layers, $\frac{\varepsilon_2}{\varepsilon_1} = 0.5$, $\zeta_1$ = $\zeta_2$, $\zeta_3$ = $\zeta_4$ = $0.5\zeta_1$, and $\frac{\sigma_2}{\sigma_1} = 0.1$.

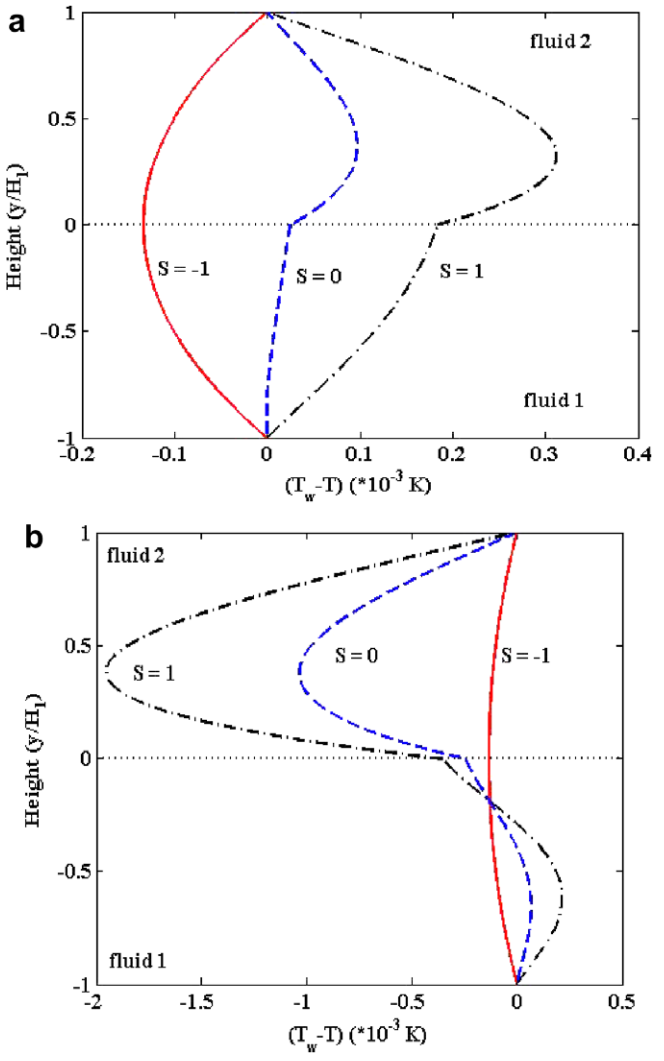


**Fig. 3.** Representative temperature profiles in the two fluid layers, for different values of S, for (a) $P = 0.05$, (b) $P = -0.05$. Other parameters are taken as mentioned in the caption of Fig. 2.

from the lower fluid layer to the upper fluid layer in the interfacial region. The fluid temperature subsequently increases in the upper layer, so as to match the thermal conditions prevailing at the upper wall. It is also noteworthy that the upper layer, being thermally less conductive than the lower one, is characterized with lower interfacial temperature gradients, to maintain the continuity of heat fluxes. For $S = 1$, heat is externally added to the fluid through the channel walls, leading to a lower fluid temperature than the wall temperature, at all locations. Stronger Joule heating effects, as such can only shift the temperature characteristics more towards the corresponding profile variation depicted for $S = 0$, without altering the qualitative trend.

Fig. 4 depicts the variations in Nusselt numbers (Nu) for the two layers, with variations in the parameters $S$ and $P$, all other parameters remaining same as before. Interestingly, the case with $S = -1$ results in the highest possible Nu value for the lower fluid layer, as compared to the other two values of $S$, whereas the contrastingly reverse trend is observed for the upper fluid layer. This can be attributed to the fact that the highest non-dimensional bottom-wall temperature gradient and the lowest non-dimensional top-wall temperature gradient is observed to occur for this value of $S$. Interestingly, for $S = 0$, a lower difference between the bulk mean temperature and the wall temperature compensates for a reduced temperature gradient at the top wall, so that the highest value of Nu in the upper fluid layer occurs for this case. For $S = 1$, on the other hand, low values of the bottom-wall temperature gradients are accompanied with higher extents of deviation of the bulk mean temperature from the wall temperature. Consequently, for such cases, the Nu value corresponding to the lower fluid layer attains a minimum. Further, for both the fluid layers, the Nu value tends to decrease with an increase in the magnitude of P (irrespective of directionality), for lower ranges of magnitude of P, corresponding to $S = 0$ and $S = 1$. This is because of the fact that an introduction of electroosmotic effects tends to elevate the advective strengths drastically, thereby attempting to nullify the wall temperature gradients. Despite that, a dynamical equilibrium between axial advection and transverse thermal diffusion promptly sets in with further increments in the magnitudes of $P$, rendering the Nu values to be virtually insensitive with the later. For $S = -1$, the conflicting influences of Joule heating and wall cooling aid in achieving this dynamical equilibrium at much lower relative strengths of the imposed electrical field, so that an apparent insensitivity of the values of Nu with respect to the magnitudes of $P$ can be observed for this case. The Nu variations, being strongly dependent on the square of the imposed electric field, exhibit much less sensitivities on the variations in $P$ as compared to the variations in the electric field strength.

Fig. 5 depicts typical variations in the values of Nusselt number for the case when the top layer is electrically non-conducting, as a function of the relative thicknesses of the individual fluid layers for $P = \pm 0.5$, all other parameters remaining unaltered. Interestingly, the values of Nu are found to increase with the thickness of the lower fluid layer for all cases, except for the value of $Nu_1$ corresponding to $S = -1$. For the later case, a thicker bottom layer trivi-

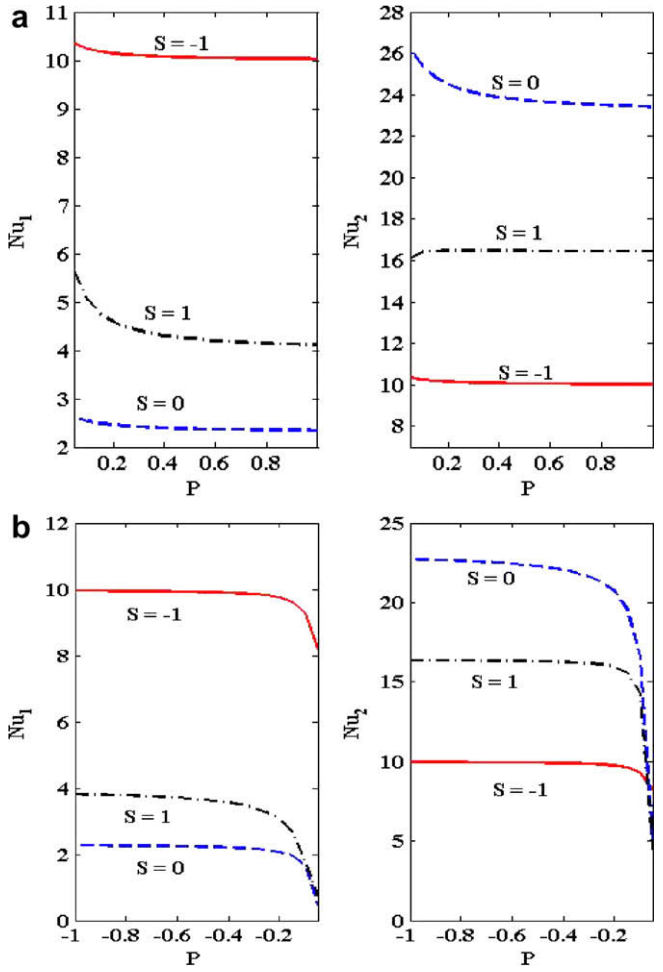


**Fig. 4.** Variations of Nusselt numbers with S, for (a) positive values of $P$, (b) negative values of $P$. Other parameters are taken as mentioned in the caption of Fig. 2.

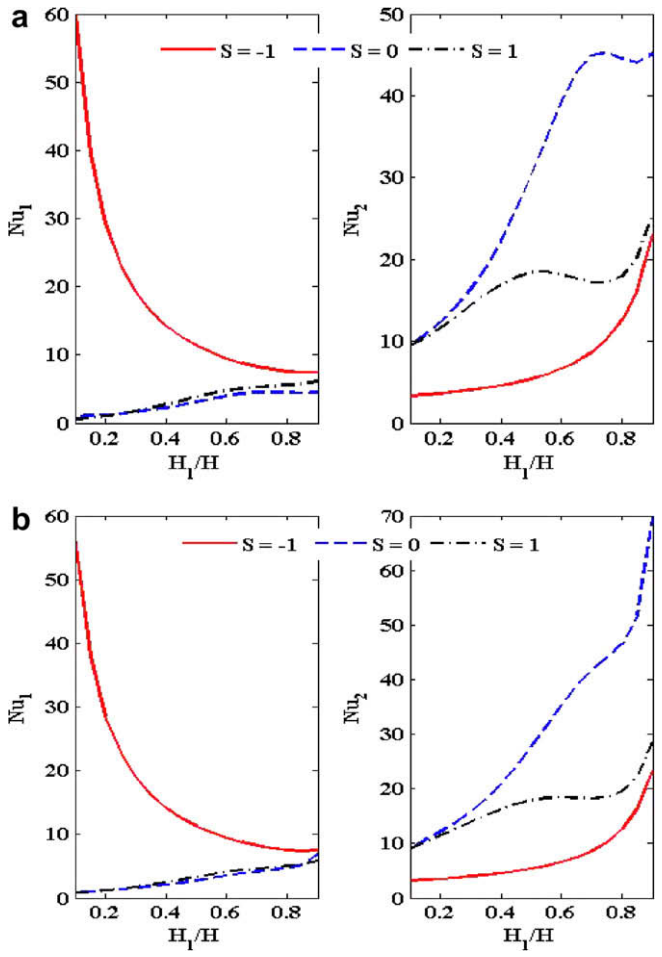


**Fig. 5.** Variations of Nusselt numbers S, as a function of interfacial position, taking (a) $P = 0.5$, (b) $P = -0.5$. Other parameters are taken as $\frac{\varepsilon_2}{\varepsilon_1} = 0$ $\zeta_1 = \zeta_2$, $\zeta_3 = \zeta_4 = 0$, $\frac{\sigma_2}{\sigma_1} = 0$.

ally implies a lower non-dimensional lower wall temperature gradient and a higher non-dimensional upper wall temperature gradient. However, for $S = 0$ and $S = 1$, the decrements in wall temperature gradients occur at a relatively slower rate as compared to the corresponding reductions in the difference between the bulk mean temperature and the wall temperature, with a thickening of the bottom layer. As a consequence, the value of $Nu_1$ increases with enhancements in the thickness of the lower fluid layer. For the electrically non-conducting upper fluid layer, decrements in the layer thickness trivially imply increments in the non-dimensional wall temperature gradients, in the absence of Joule heating effects (because of the electrically non-conducting fluid). Accordingly, the value of $Nu_2$ increases monotonically with reductions in the thickness of this layer, for all cases.

## 4. Conclusions

A theoretical model has been established in this study for fully developed convective heat transfer in two immiscible fluid layers confined within parallel plate microchannels subjected to electroosmotic effects. The velocity and temperature distributions in the two fluid layers have been obtained analytically, under constant wall heat flux conditions. It has also been verified (not detailed in the manuscript for brevity) that the analytical solutions agree excellently with more involved full-scale numerical solution predictions. The upper fluid layer has been assumed to be weakly conducting, as compared to the lower one. It has been revealed that the highest value of the Nusselt number corresponding to the bottom fluid layer occurs when the channel walls are cooled, whereas the same in the top fluid layer occurs when the external heat fluxes to the walls are effectively zero. The case with wall cooling is characterized with a decrement in the Nusselt number corresponding to the bottom fluid (electrically more conducting layer) with a thickening of its lateral extent, whereas for all other cases the Nusselt number increases with increments in the conducting layer thickness.

## References

[1] S. Das, S. Chakraborty, On use of transverse electrodes for improved DNA hybridization in microchannels, AIChE J. 53 (2007) 1086–1099.
[2] S. Chakraborty, D. Pal, Microchannel flow control through a combined magneto-electro-hydrodynamic transport, J. Phys. D 39 (2006) 5364–5371.
[3] S. Chakraborty, Augmentation of peristaltic microflows through electroosmotic mechanisms, J. Phys. D 39 (2006) 5356–5363.
[4] R.J Hunter, Zeta Potential in Colloid Science, Academic, San Diego, 1981.
[5] S. Das, K. Subramanian, S. Chakraborty, Analytical investigations on the effects of substrate kinetics on macromolecular transport and hybridization through microfluidic channels, Colloids Surf. B 58 (2007) 203–217.
[6] G.D. Ngoma, F. Erchiqui, Pressure gradient and electroosmotic effects on two immiscible fluids in a microchannel between two parallel plates, J. Micromech. Microeng. 16 (2006) 83–91.
[7] Y. Gao, T.N. Wong, C. Yang, K.T. Ooi, Two-fluid electroosmotic flow in microchannels, J. Colloid Interf. Sci. 284 (2005) 306–314.
[8] Y. Gao, T.N. Wong, C. Yang, N.T. Nguyen, K.T. Ooi, C. Wang, Theoretical investigation of two-fluid electroosmotic flow in microchannels, J. Phys. 34 (2006) 470–474.
[9] Y. Gao, T.N. Wong, J.C. Chai, C. Yang, K.T. Ooi, Numerical simulation of two-fluid electroosmotic flow in microchannels, Int. J. Heat Mass Transfer 48 (2005) 5103–5111.
[10] P.J. Stiles, D.F. Fletcher, Hydrodynamic control of the interface between two liquids flowing through a horizontal or vertical microchannel, Lab Chip 4 (2004) 121–124.
[11] S. Das, S. Chakraborty, Augmentation of macromolecular adsorption rates through transverse electric fields generated across patterned walls of a microfluidic channel, J. Appl. Phys. 100 (2006) 014098.
[12] S. Das, T. Das, S. Chakraborty, Modeling of coupled momentum, heat and solute transport during DNA hybridization in a microchannel in presence of electroosmotic effects and axial pressure gradients, Microfluid. Nanofluid. 2 (2006) 37–49.
[13] K. Horiuchi, P. Dutta, Joule heating effects in electroosmotically driven microchannel flows, Int. J. Heat Mass Transfer 47 (2004) 3085–3095.
[14] S. Das, S. Chakraborty, Analytical solutions for velocity, temperature and concentration distribution in electroosmotic microchannel flows of a non-newtonian bio-fluid, Anal. Chim. Acta 559 (2006) 15–24.
[15] S. Das, T. Das, S. Chakraborty, Analytical solutions for rate of DNA hybridization in a microchannel in presence of pressure-driven and electroosmotic flows, Sensors Actuators B 114 (2006) 957–963.
[16] A. Sharma, S. Chakraborty, Semi-analytical solution of the extended Graetz problem for combined electroosmotically and pressure driven microchannel flows with step-change in wall temperature, Int. J. Heat Mass Transfer 51 (2008) 4875–4885.